Design of chemically propelled nanodimer motors

Yu-Guo Tao[a] and Raymond Kapral[b]
Chemical Physics Theory Group, Department of Chemistry, University of Toronto, Ontario M5S 3H6, Canada

(Received 7 February 2008; accepted 21 March 2008; published online 28 April 2008)

The self-propelled motion of nanodimers fueled by a chemical reaction taking place under nonequilibrium steady state conditions is investigated. The nanodimer consists of a pair of catalytic and chemically inactive spheres, in general with different sizes, with a fixed internuclear separation. The solvent in which the dimer moves is treated at a particle-based mesoscopic level using multiparticle collision dynamics. The directed motion of the dimer can be controlled by adjusting the interaction potentials between the solvent molecules and the dimer spheres, the internuclear separation, and sphere sizes. Dimers can be designed so that the directed motion along the internuclear axis occurs in either direction and is much larger than the thermal velocity fluctuations, a condition needed for such nanodimers to perform tasks involving targeted dynamics. © *2008 American Institute of Physics*. [DOI: 10.1063/1.2908078]

I. INTRODUCTION

The conversion of chemical energy into directed motion on the nanoscale is widespread in nature. Biological molecular motors, such as kinesin and ATPsynthase, play essential roles in the transport and synthesis biochemicals in the cytoplasm and in cell motility.[1–3] Such molecular motors operate in the low Reynolds number regime,[4] usually through chemically induced symmetry-breaking conformational changes.

In addition to these biochemical motors, synthetic molecular motors have been designed that use chemical, light, or other energy sources to perform directed motion.[5–14] Many of these synthetic motors also rely on asymmetric molecular motions for propulsion. Another class of synthetic motors has been constructed that does not depend on conformational changes for their operation. This class of motors includes electrochemically synthesized striped bimetallic nanorods[15–23] and synthetic catalytic molecules tethered to inactive particles.[8] The bimetallic nanorod consists of platinum (or nickel) and gold segments and is immersed in a hydrogen peroxide aqueous solution that provides the fuel for the motion as result of chemical decomposition that occurs at the Pt (or Ni) catalytic end. A number of mechanisms for the propulsion have been proposed.[16,17,23] In parallel with these synthetic approaches to the construction of molecular motors, simple theoretical and computational models have been proposed that capture features essential to self-propelled motion.[24–29]

Models for self-propelled nanoparticle motion are often based on continuum descriptions of the solvent in which they move and on macroscopic descriptions of the propulsion mechanism, such as surface tension gradients, diffusiophoretic effects, etc. Microscopic[26] and mesoscopic[27,28] simulations of model motors and swimmers have been carried out which do not require such assumptions. In this article we consider a model for chemically powered nanodimers that perform directed motion; however, previously only small velocities were achieved, which were masked by thermal fluctuations unless extensive averaging was carried out.[28] In this article we discuss the factors that control the nanodimer velocity and show how dimers can be designed to have velocities that are larger than the thermal fluctuations, leading to easily observed directed motion. Such strongly directed motion is required for applications where synthetic motors may possibly be used to target specific regions or perform specific tasks, as opposed to simply enhancing the diffusion coefficient of the motor.

In Sec. II we describe the mesoscopic model for the dimer and solvent. The important features of the model are the particle-based treatment of the solvent using multiparticle collision (MPC) dynamics[30–32] that captures most essential features of full molecular dynamics, and the fact that interactions between the dimer monomers and solvent molecules occur through intermolecular forces. As a result, a molecular-based description of the propulsion mechanism can be given. Section III describes the dynamics of a nanodimer executing rapid directed motion, along with the solvent velocity and concentration fields, that play important parts in the mechanism for the motion. An analysis of the principal factors that control the nanodimer motion are discussed in Sec. IV in terms of the forces responsible for the motion. Simulation results for a variety of system parameters are presented in Sec. V that show how various dimer geometrical and energetic factors influence the motion. The conclusions of the study are given in Sec. VI.

II. NANODIMER MODEL

The model nanodimer[28] consists of a catalytic sphere C with diameter d_C and a noncatalytic sphere N with diameter d_N, separated by a fixed internuclear distance R. The irreversible chemical reaction, $A+C \rightarrow B+C$, occurs at the catalytic C sphere with probability p_R whenever A encounters C.[33]

[a]Electronic mail: ytao@chem.utoronto.ca.
[b]Electronic mail: rkapral@chem.utoronto.ca.

The solvent is modeled by a large number $N_s=N_A+N_B$, typically 10^5-10^6, of pointlike A and B molecules with identical masses m, with continuous positions and velocities, $(\mathbf{r}_i,\mathbf{v}_i;i=1,\ldots,N_s)$.

The solvent A molecules interact with both the C and N spheres through repulsive Lennard–Jones (LJ) potentials,

$$V_{\mathrm{LJ}}^{R}(r)=4\epsilon_A\left[\left(\frac{\sigma_S}{r}\right)^{12}-\left(\frac{\sigma_S}{r}\right)^{6}+\frac{1}{4}\right],\quad r\le r_c, \tag{1}$$

with energy ϵ_α, $(\alpha=A,B)$, and distance σ_S, $(S=C,N)$, parameters; the cutoff distance is $r_c=2^{1/6}\sigma_S$. The B molecules interact with the catalytic C sphere through the same repulsive LJ potential as in Eq. (1), but interact with the noncatalytic N sphere through either a repulsive LJ potential with a different energy parameter, ϵ_B, or a truncated attractive LJ potential,

$$V_{\mathrm{LJ}}^{A}(r)=4\epsilon_B\left[\left(\frac{\sigma_S}{r}\right)^{12}-\left(\frac{\sigma_S}{r}\right)^{6}\right]\begin{cases}1, & r\le r_t,\\ S(r), & r_t<r\le r_c,\end{cases} \tag{2}$$

where $S(r)$ is a switching function to smoothly truncate the potential[34]

$$S(r)=1-\frac{(r-r_t)^2(3r_c-2r-r_t)}{(r_c-r_t)^3}. \tag{3}$$

We take $r_t=1.1688\sigma_S$ and $r_c=1.3636\sigma_S$.

The time evolution of the system is carried out using a mesoscopic hybrid molecular dynamics-multiparticle collision (MD-MPC) dynamics scheme.[30–32] The pointlike solvent molecules evolve by MPC dynamics, which consists of a streaming step and a collision step. In the streaming step, within a time interval τ, the motions of all particles, the nanodimer and solvent molecules, are governed by Newton's equations of motion. In the collision step, multiparticle collisions occur among the solvent A and B particles. To carry out such multiparticle collisions, the system partitioned into a cubic lattice I of cells with cell size a_0, and collisions occur independently in each cell. The velocity of each particle i in a cell, relative to the center-of-mass velocity $\mathbf{V}_{\mathrm{cm},I}$ of the cell, is rotated about a randomly chosen axis by a fixed angle α,

$$\mathbf{v}_i'(t+\tau)=\mathbf{V}_{\mathrm{cm},I}+\hat{\omega}(\alpha)[\mathbf{v}_i(t+\tau)-\mathbf{V}_{\mathrm{cm},I}], \tag{4}$$

where $\hat{\omega}(\alpha)$ is a rotation matrix, chosen at random from a set of rotation matrices, and $\mathbf{v}_i'(t+\tau)$ is the postcollision velocity of particle i. Random shifts of the grid defining the collision cells are also applied in each direction, so that Galilean invariance is ensured even in the case of small mean free paths.[35,36] This collision step eliminates the need to compute the time-consuming direct interactions among A and B species. The dynamics is microcanonical, satisfies mass, momentum, and energy conservation, and preserves phase space volumes, all attributes of full molecular dynamics. As a result, hydrodynamic interactions, which are important for the nanodimer dynamics, are taken into account properly.

In our simulations, all quantities are reported in dimensionless LJ units based on energy ϵ, mass m, and distance σ parameters: $r/\sigma\to r$, $t(\epsilon/m\sigma^2)^{1/2}\to t$ and $k_BT/\epsilon\to T$. The nanodimer is dissolved in a solvent of A and B molecules within a cubic box of volume V with periodic boundary conditions. The simulation box was then subdivided into $(L_b)^3$ cells in order to perform multiparticle collisions. The rotation angle was fixed at $\alpha=90°$. We chose an average number density of $n_0\approx 9.2$ in all simulations; thus, for example, the total number of solvent particles is $\approx 10^6$ in a system with $(48)^3$ collision cells. The masses of both A and B species were taken to be $m=1$, while the masses of the C and N spheres were adjusted according to their volumes to ensure that the dimer was approximately neutrally buoyant. The MD time step used to integrate Newton's equations of motion with the velocity Verlet algorithm was $\Delta t=0.01$, while the multiparticle collision time ranged from $\tau=0.1$ to 1.0. The system temperature varied from $T=1/12$ to 2/3. To prevent discontinuous potential changes when the $A\to B$ reaction occurs, the internuclear separation R was fixed by a holonomic constraint[37,38] in the equation of motion. The LJ potential parameter was chosen to be $\epsilon_A=1.0$ in most of the simulations, while ϵ_B varied from 0.1 to 10.0 to change both the speed and direction of the movement of the dimer.

III. NANODIMER DYNAMICS

Before discussing the mechanism of nanodimer motion and presenting results pertaining to the design of nanodimers with specific propulsion properties, we give an example of the dimer and solvent motions under nonequilibrium steady state conditions. Since the reaction $A\to B$ is assumed to be irreversible, in the absence of fluxes of chemical reagents eventually all A molecules would be converted to B molecules and self-propelled motion would cease. Fluxes of these species are introduced in order to maintain the motion under steady state conditions. Starting from an initial state containing all A molecules, the system is allowed to reactively evolve and whenever a B molecule diffuses to a prescribed distance sufficiently far from the dimer it is converted to A, mimicking fluxes of these species into and out of the system that maintain the A concentration at a fixed value far from the dimer. Under the resulting steady state conditions self-propulsion continues indefinitely, facilitating its statistical characterization.

Figure 1(a) shows an instantaneous configuration of both A and B solvent molecules in the vicinity of an asymmetric nanodimer in the steady state regime. The inhomogeneous nonequilibrium B particle density field in the vicinity of the noncatalytic sphere plays an important role in the propulsion mechanism. The form of this density field is shown in Figs. 1(b) and 1(c). Figure 1(b) shows an instantaneous configuration of the solvent molecules in a $24\times 16\times 2$ slice parallel to the dimer internuclear axis. While total solvent molecule density field is approximately uniform, the gradient of the B molecule field in the vicinity of the dimer is evident. This density gradient is seen more clearly in Fig. 1(c), which shows that the average B density field varies from high to low as one traverses the dimer from the catalytic to noncatalytic ends.

The fluid flow field induced by dimer motion is also important for the propulsion mechanism. The local solvent velocity field in the vicinity of dimer is plotted in Fig. 2. Collective hydrodynamic effects that emerge from the

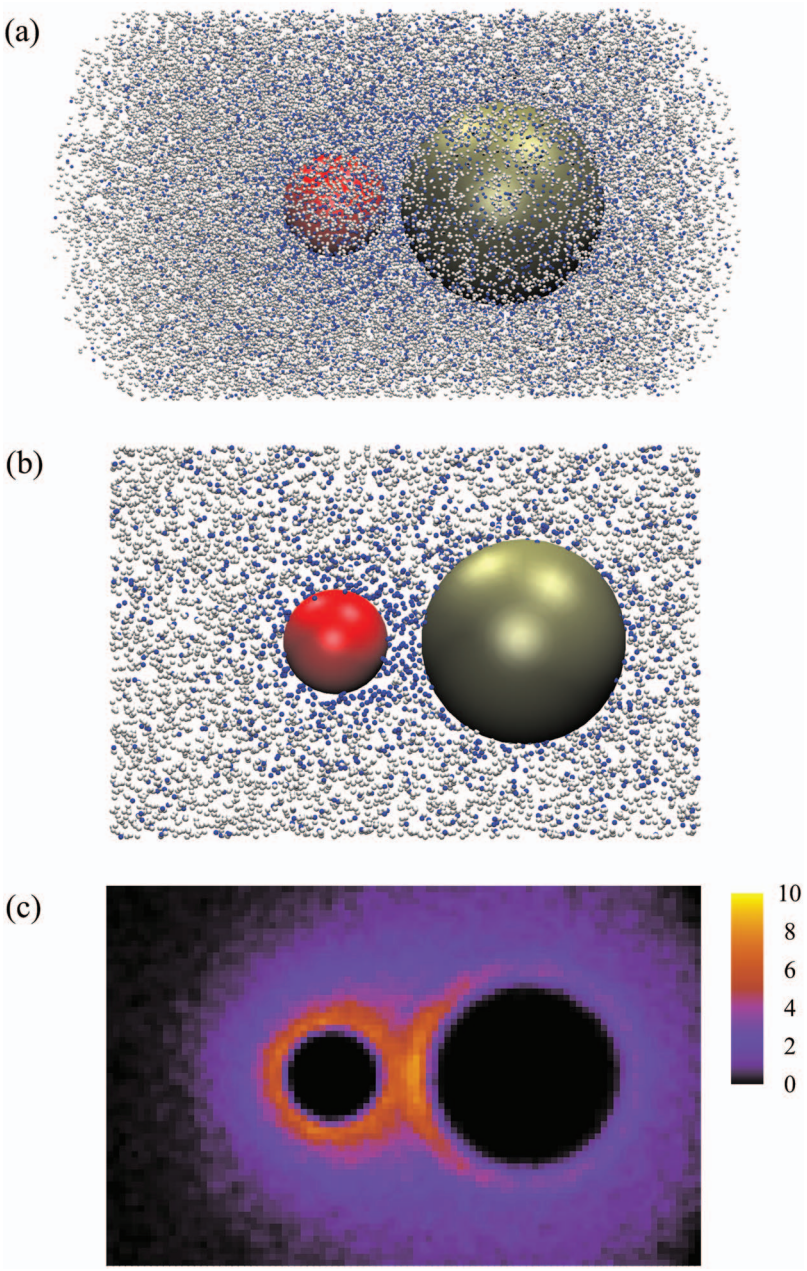

FIG. 1. (Color) (a) Instantaneous configuration of A (white) and B (blue) molecules in the vicinity of the nanodimer. The simulation was carried out in a $48\times48\times48$ cubic box. The diameter of the catalytic (red) and the noncatalytic (brown) spheres are 4.0 and 8.0, respectively. Repulsive LJ interactions between the solvent molecules and dimer spheres were used, with $\epsilon_A=1.0$ and $\epsilon_B=0.1$ for A and B molecules, respectively. Other parameters are $T=1/6$ and $\tau=0.5$. (b) Instantaneous configuration of solvent molecules in a $24\times16\times2$ slice parallel to the nanodimer internuclear axis. (c) The average number density profile of B molecules in the vicinity of the nanodimer for the slice shown in (b).

particle-based MPC dynamics at small scales manifest themselves in the solvent "backflow" seen at the rear of the large noncatalytic sphere. The dimer moves in the direction of the small catalytic sphere and collective hydrodynamic effects enhance this motion. Such collective effects have their origin in the coupling between the dimer velocity and the fluid viscous modes. Similar effects have been observed in early molecular dynamics simulations of the velocity correlation function and are responsible for the long time tails seen in this function.[39]

Figure 3 is an example of a trajectory of the self-propelled dimer. One can see that for this particular dimer the component velocity along the dimer internuclear axis V_z is much larger than the components in the transverse directions (see also the inset in Fig. 3). The average center-of-mass velocity of the dimer projected along the instantaneous internuclear axis is $V_z\equiv\langle\mathbf{V}(t)\cdot\hat{\mathbf{R}}(t)\rangle\approx0.056$, where the angle

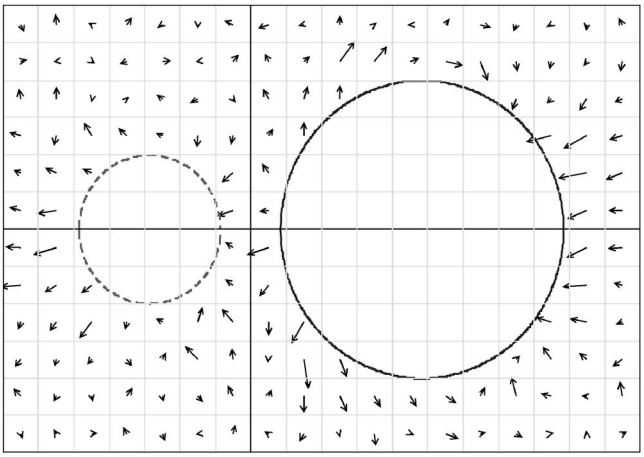

FIG. 2. Solvent molecule velocity field near the dimer spheres, which are separated by a fixed internuclear distance of $R=7.7$. The system is as same as that described in Fig. 1.

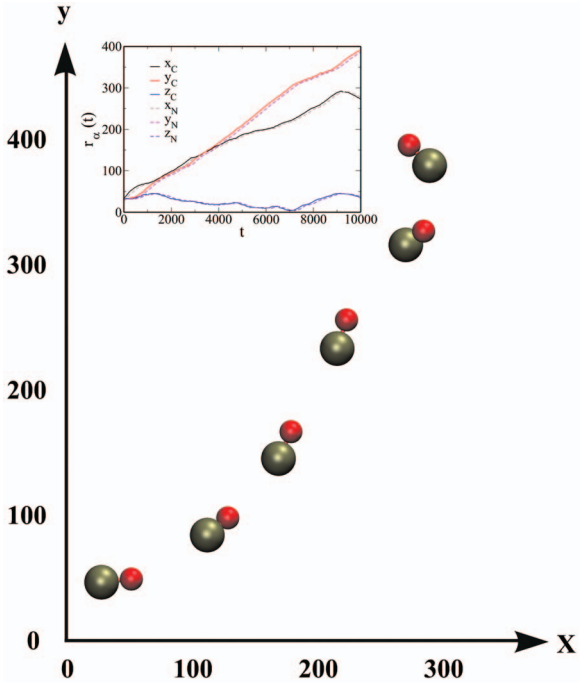

FIG. 3. (Color) Trajectory of the self-propelled nanodimer. Motion occurs in the direction of the catalytic end along its internuclear axis. The time interval between each frame is 2000. The simulation was carried out in a $64\times64\times64$ cubic box with a total number of 2 400 000 A and B solvent molecules. The A molecules interact with both spheres of the dimer through repulsive LJ potentials with $\epsilon_A=1.0$, while the B molecules interact with the noncatalytic monomer through an attractive LJ potential with $\epsilon_B=0.1$. Other parameters are as same as those in Fig. 1(a). The inset plots the three components of the positions of the catalytic (solid) and noncatalytic (dashed) spheres as a function of time.

brackets denote a time average. The translational D_t and rotational D_r diffusion coefficients can be calculated by computing the mean square displacement and autocorrelation function of the unit vector along the internuclear axis, respectively. These transport coefficients are found to be $D_t \approx 1.6$ and $D_r \approx 0.00018$. The orientational relaxation time τ_θ can be determined from D_r and is $\tau_\theta=(2D_r)^{-1}=2800$. Given the value of V_z we see that the dimer will move about 20 times its length on average before reorientation occurs. Hence, for these dimer parameters there is strong directed motion. Consequently, the directed movement is not masked by Brownian translational and rotational motions.

IV. PROPULSION MECHANISM

The basic elements that are responsible for directed motion are the different interaction potentials of chemical species with the two monomers in the dimer and the nonequilibrium concentration gradients produced by the chemical reaction at the catalytic end of the dimer. In order to design nanodimers with different propulsion properties, it is important to understand the geometrical and the dynamical factors that influence these two components. Since our nanodimer and solvent models are particle-based, the effects of variations in dimer size, dimer-solvent interaction potentials, temperature, solvent properties, and chemical gradients can be examined in detail. We base our analysis on the formulation outlined in Ref. 28, generalized to asymmetric situations and different potential interactions.

We use $\mathbf{r}$ to denote coordinates measured with the catalytic C sphere as the origin, while $\hat{\mathbf{z}}$ denotes the unit vector along the dimer internuclear bond, pointing in the direction of the noncatalytic N sphere. The $\mathbf{r}'$ coordinate, defined with the noncatalytic N sphere as the origin, is related to $\mathbf{r}$ by $\mathbf{r}'=\mathbf{r}-R\hat{\mathbf{z}}$. The total LJ potential of the system is

$$V(\mathbf{r}^{N_A},\mathbf{r}^{N_B})=\sum_{\alpha=A}^{B}\sum_{i=1}^{N_\alpha}[V_{C\alpha}(r_{i\alpha})+V_{N\alpha}(r'_{i\alpha})], \tag{5}$$

where $\mathbf{r}^{N_\alpha}=(\mathbf{r}_{1\alpha},\mathbf{r}_{2\alpha},\ldots,\mathbf{r}_{N_\alpha\alpha})$ and $\mathbf{r}_{i\alpha}$ is the vector distance to solvent molecule i of species α and $r_{i\alpha}$ its magnitude. Here $r'_{i\alpha}=|\mathbf{r}_{i\alpha}-R\hat{\mathbf{z}}|$. The instantaneous force along the dimer axis is then given by

$$\hat{\mathbf{z}}\cdot\mathbf{F}=-\sum_{\alpha=A}^{B}\sum_{i=1}^{N_\alpha}\left[(\hat{\mathbf{z}}\cdot\hat{\mathbf{r}}_{i\alpha})\frac{dV_{C\alpha}(r_{i\alpha})}{dr_{i\alpha}}+(\hat{\mathbf{z}}\cdot\hat{\mathbf{r}}'_{i\alpha})\frac{dV_{N\alpha}(r'_{i\alpha})}{dr'_{i\alpha}}\right]. \tag{6}$$

Our interest is in the average force along the bond in the nonequilibrium steady state $\langle\hat{\mathbf{z}}\cdot\mathbf{F}\rangle$, whose computation involves a knowledge of the local average density in the steady state. Introducing the microscopic local density field $\rho_\alpha(\mathbf{r};\mathbf{r}^{N_\alpha})=\Sigma_{i=1}^{N_\alpha}\delta(\mathbf{r}_{i\alpha}-\mathbf{r})$ of species α, and its nonequilibrium steady state average, $\rho_\alpha(\mathbf{r})=\langle\rho_\alpha(\mathbf{r};\mathbf{r}^{N_\alpha})\rangle$, we may write the average force as

$$\langle\hat{\mathbf{z}}\cdot\mathbf{F}\rangle=-\sum_{\alpha=A}^{B}\int d\mathbf{r}\rho_\alpha(\mathbf{r})(\hat{\mathbf{z}}\cdot\hat{\mathbf{r}})\frac{dV_{C\alpha}(r)}{dr}-\sum_{\alpha=A}^{B}\int d\mathbf{r}\rho_\alpha(\mathbf{r})(\hat{\mathbf{z}}\cdot\hat{\mathbf{r}})\frac{dV_{N\alpha}(\mathbf{r}')}{dr'}. \tag{7}$$

A knowledge of the density field $\rho_\alpha(\mathbf{r})$ is an essential ingredient in the computation of the nanodimer velocity. For a system in equilibrium the local density field is given by

$$\rho_\alpha^{\mathrm{eq}}(\mathbf{r})=\langle\rho_\alpha(\mathbf{r};\mathbf{r}^{N_\alpha})\rangle_{\mathrm{eq}}=n_\alpha e^{-\beta[V_{C\alpha}(r)+V_{N\alpha}(r')]}, \tag{8}$$

where the angle brackets $\langle\cdots\rangle_{\mathrm{eq}}$ signify an equilibrium canonical average and the equilibrium number density is $n_\alpha=N_\alpha^{\mathrm{eq}}/V$. The last line of this equation follows from the fact that the total potential energy of the system has the form given in Eq. (5). If this expression for $\rho_\alpha^{\mathrm{eq}}(\mathbf{r})$ is substituted into Eq. (7), we see that the average force is zero in view of the angular integrations. This confirms that dimer directed motion is a nonequilibrium effect that relies on the form of the concentration gradient produced by the chemical reaction. Given this form of the equilibrium density, in the steady state it is convenient to define the local steady state density $n_\alpha(\mathbf{r})$ by $\rho_\alpha(\mathbf{r})=n_\alpha(\mathbf{r})e^{-\beta[V_{C\alpha}(r)+V_{N\alpha}(r')]}$. Using this form for the steady state density in Eq. (7), taking into account that $V_{CA}=V_{CB}$ for our model nanodimer and neglecting fluctuations in the local total solvent density, we have

$$\langle \hat{\mathbf{z}} \cdot \mathbf{F} \rangle = -\int d\mathbf{r} n_A(\mathbf{r}) e^{-\beta[V_{CA}(r)+V_{NA}(r')]} (\hat{\mathbf{z}} \cdot \hat{\mathbf{r}}') \frac{dV_{NA}(r')}{dr'} - \int d\mathbf{r} n_B(\mathbf{r}) e^{-\beta[V_{CB}(r)+V_{NB}(r')]} (\hat{\mathbf{z}} \cdot \hat{\mathbf{r}}') \frac{dV_{NB}(r')}{dr'}. \tag{9}$$

A further simplification of this equation is possible. Since the repulsive LJ potentials with the catalytic sphere are cutoff at $2^{1/6}\sigma_C$ and the dimer internuclear separation long enough to prevent discontinuous potential changes when the chemical reaction occurs, the terms involving $V_{CA}(r)$ and $V_{CB}(r)$ in Eq. (9) do not contribute to the mean force.

In the steady state, the force arising from nonequilibrium chemical reactions is balanced by the frictional force $-\zeta V_z$ on the dimer, where ζ is the friction coefficient of the dimer center of mass. Thus, the steady state velocity is given by

$$V_z = \frac{k_B T}{\zeta} \langle \hat{\mathbf{z}} \cdot \beta \mathbf{F} \rangle = \frac{k_B T}{\zeta} \left[\int d\mathbf{r}' n_A(|\mathbf{r}' + R\hat{\mathbf{z}}|)(\hat{\mathbf{z}} \cdot \hat{\mathbf{r}}') \frac{de^{-\beta[V_{NA}(r')]}}{dr'} + \int d\mathbf{r}' n_B(|\mathbf{r}' + R\hat{\mathbf{z}}|)(\hat{\mathbf{z}} \cdot \hat{\mathbf{r}}') \frac{de^{-\beta[V_{NB}(r')]}}{dr'} \right], \tag{10}$$

where we have changed the origin for the integration using the change of variables $\mathbf{r}=\mathbf{r}'+R\hat{\mathbf{z}}$. Use of this expression to compute the dimer velocity requires knowledge of the friction coefficient and the steady state density field.

The friction coefficient may be estimated as follows: For a single Brownian particle in a mesoscopic solvent,[40] the friction which accounts for both microscopic and hydrodynamic contributions can be written approximately as $\zeta_S^{-1} = \zeta_m^{-1} + \zeta_h^{-1}$ with

$$\zeta_m = \frac{8}{3}\rho\sigma_S^2\sqrt{2\pi m k_B T}, \quad \zeta_h = 4\pi\eta\sigma_S, \tag{11}$$

where ρ is the number density of the solvent and η denotes the viscosity of the MPC solvent. Neglecting hydrodynamic interactions, the friction coefficient of the dimer center-of-mass is given by the sum of the friction coefficients of the two monomers $\zeta=\zeta_C+\zeta_N$. The effects of hydrodynamic interactions can be approximately accounted for by assuming Oseen interactions between the two spheres, in which case we have the space-dependent friction tensor,[41,42]

$$\zeta(\mathbf{R}) = (\zeta_0^{-1} + \mathbf{T}(\mathbf{R}))^{-1}, \tag{12}$$

where ζ_0 is the diagonal one-particle friction tensor, whose diagonal elements are ζ_S, $(S=C,N)$, and $\mathbf{T}(\mathbf{R})$ is the Oseen tensor,

$$\mathbf{T}_{\alpha\beta}(\mathbf{R}) = (1-\delta_{\alpha\beta})\frac{1}{8\pi\eta R}(\mathbf{I} + \hat{\mathbf{z}}\hat{\mathbf{z}}). \tag{13}$$

From this expression the zz component of the center-of-mass friction coefficient can be computed to give

$$\zeta(R) = \frac{\zeta_C + \zeta_N - 4\zeta_C\zeta_N\phi(R)}{1 - 2\zeta_C\zeta_N\phi^2(R)}, \tag{14}$$

where $\phi = 1/(8\pi\eta R)$.

The computation of the friction coefficient requires knowledge of the solvent shear viscosity. In MPC dynamics, the viscosity consists two contributions:[43,44] The kinetic viscosity from the momentum transferred during the free streaming step and the collisional viscosity from the momentum transferred during the velocity rotations. The viscosity is given by $\eta = \eta_{\text{kin}} + \eta_{\text{col}}$, where

$$\eta_{\text{kin}} = \frac{\gamma k_B T \tau}{a_0^3}\left[\frac{5\gamma}{(\gamma - 1 + e^{-\gamma})(4 - 2\cos\alpha - 2\cos 2\alpha)} - \frac{1}{2}\right], \tag{15}$$

$$\eta_{\text{col}} = \frac{m(1-\cos\alpha)}{18 a_0 \tau}(\gamma - 1 + e^{-\gamma}),$$

where γ is the number of particles per collision cell.

The computation of the steady state density $n_\alpha(\mathbf{r})$ is more difficult due to the presence of the noncatalytic sphere. A crude estimate for this density can be obtained by assuming the density can be obtained from the solution of the diffusion equation with a radiation boundary condition to account for reaction, and neglecting the presence of the noncatalytic sphere so that spherical symmetry can be assumed for the solution of the diffusion equation. Under these conditions the steady state solution of the of the diffusion equation yields

$$n_A(r) = n_A^0\left(1 - \frac{k_{f0}}{k_{f0}+k_D}\frac{R_0}{r}\right), \quad n_B(r) = n_A^0\frac{k_{f0}}{k_{f0}+k_D}\frac{R_0}{r}, \tag{16}$$

where the reaction rate constant $k_{f0} = p_R\sigma_C^2\sqrt{8\pi k_B T/m}$ and characterizes the reactive events that occur within a diffusive boundary layer around the catalytic sphere, and the diffusion-limit Smoluchowski rate constant is $k_D = 4\pi R_0 D_A$.[45] The diffusion coefficient of A molecules, D_A, is given by

$$D_A = \frac{k_B T \tau}{2m}\left(\frac{3\gamma}{(\gamma - 1 + e^{-\gamma})(1-\cos\alpha)} - 1\right). \tag{17}$$

The reaction distance R_0 is chosen equal to the cutoff distance of the repulsive LJ potential $R_0 = 2^{1/6}\sigma_C$.

Substituting Eqs. (16) into Eq. (10) we find

$$V_z = -\frac{k_B T}{\zeta} R_0 n_A^0 \frac{k_{f0}}{k_{f0}+k_D}\int d\mathbf{r}' \frac{\hat{\mathbf{z}} \cdot \hat{\mathbf{r}}'}{|\mathbf{r}' + R\hat{\mathbf{z}}|} \times \frac{d}{dr'}[e^{-\beta V_{NA}(r')} - e^{-\beta V_{NB}(r')}]. \tag{18}$$

This expression can be simplified to make the dependence of the dimer velocity on system parameters more explicit. Performing the angular integration analytically and using the nonequilibrium density field only outside the boundary layer surrounding the noncatalytic sphere, we obtain

$$V_z = -\frac{8\pi}{3}\frac{k_B T}{\zeta} n_A^0 \frac{R_0(2^{1/6}\sigma_N^3)}{R^2}\frac{k_{f0}}{k_{f0}+k_D} \times\left[\int_0^{u_c} duue^{-\beta V_{NA}(u)} - \int_0^{u_c} duue^{-\beta V_{NB}(u)}\right], \quad (19)$$

where the reduced cutoff distance $u=r\sigma_N$ and u_c equals $2^{1/6}$ and 1.3636 for repulsive and attractive LJ potentials, respectively. The radial integrals depend only on the temperature T and the energy parameter ϵ and can be easily evaluated numerically. The use of the simple expression for the nonequilibrium density field in Eqs. (16) is perhaps the most serious approximation in this analysis. While it limits the use of Eq. (19) for quantitative predictions in some regimes, as we shall see it captures all qualitative trends seen in the simulations.

V. SIMULATION RESULTS

Equation (19) allows one to understand how the dimer velocity depends on geometric factors such as the dimer bond length R and the sphere radii, the interactions between the dimer spheres and the solvent, and the temperature and solvent viscosity. In this section, we present the results of simulations and show how these factors can be used to tune the dimer dynamics. The Reynolds number measures the relative importance of inertial and viscous forces in the dimer motion and varies in the range $\mathrm{Re}\approx 0.03-1.6$ for the dimers discussed later.

The reduced temperature, $k_BT/\epsilon \to T$, controls the magnitude of the thermal fluctuations in the system, provides the scale for the dimer-solvent interactions, and enters the reaction rate constant and the friction coefficient. We consider the nanodimer dynamics at four different temperatures: $T=2/3$, 1/3, 1/6, and 1/12. In all simulations $\epsilon_A=1.0$. Two values of ϵ_B were considered: $\epsilon_B=0.5$ where the self-propelled motion is in the direction of the catalytic sphere, and $\epsilon_B=5.0$ where the nanodimer moves in the direction of the noncatalytic sphere. All simulations were carried out in a $32\times32\times32$ cubic box. The sphere diameters are $d_C=d_N=4.0$ and the mass of each monomer is 320.0, yielding an approximately neutrally buoyant dimer.

The results are shown in Table I (top section). The simulation results were obtained by fitting the probability distribution function $p(V_z)$ to a Maxwell–Boltzmann distribution, while the theoretical predictions were obtained using Eq. (19). While not quantitatively accurate, the model is able to predict the magnitudes and trends of the nanodimer velocity. The velocity is greatest for the highest temperature $T=2/3$, but the probability distribution $p(V_z)$ has the largest dispersion. Henceforth, we consider systems with $T=1/6$. In these examples, thermal fluctuations dominate the dynamics of the nanodimer. Notice that the direction of the dimer motion can be changed from "forward" to "reverse" as ϵ_B varies. When $\epsilon_B > \epsilon_A$, the integral in Eq. (19) is positive, indicating that the nanodimer moves in the direction of the noncatalytic sphere.

The nonequilibrium A and B particle density fields in the vicinity of the noncatalytic sphere depend on the internuclear separation R and, from Eq. (19), we see that V_z is inversely proportional to R^2. Figure 4 shows results of simulations of nanodimers with various internuclear separations ranging from 4.5 to 6.0. In these simulations, the diameters of both spheres are chosen to be equal, $d_C=d_N=4.0$. The velocity probability distribution functions, $p(V_z)$, are shown in Fig. 4(a), while the running averages of the dimer velocity, $\langle V_z\rangle(t)$, (the angle brackets denote an average over 100 realizations) are shown in Fig. 4(b). The average velocity of the dimer along the internuclear axis is considerably smaller than its dispersion: The motion is strongly influenced by fluctuations. The discrepancy with the model calculations is largest when the internuclear separation is smallest. This is likely due to the errors in the nonequilibrium density fields in Eq. (16) that result from the neglect of the noncatalytic sphere in the solution of the diffusion equation. The R dependence of the friction coefficient yields only a small contribution in this regime.

TABLE I. Average velocities of the center-of-mass of the nanodimer along its internuclear axis. Results in the top part of the table show V_z as a function of temperature. Parameters are $d_C=d_N=4.0$, $R=4.5$, $\epsilon_B=0.5$ (the first two lines) and 5.0 (the last two lines), respectively. The middle part of the table shows how changes in the internuclear separation influence V_z. Parameters are $d_C=d_N=4.0$, $\epsilon_B=5.0$, and $T=1/6$. The bottom part of the table shows V_z for different noncatalytic sphere diameters for $d_C=4.0$, $\epsilon_B=0.1$, and $T=1/6$. Internuclear separations are chosen to be as close as possible given the sphere diameters $R=4.5$, 5.1, 6.0, and 6.8 for nanodimers with the d_N values given in the table.

T	2/3	1/3	1/6	1/12
Simulation	0.0042	0.0036	0.0024	0.0016
Theory	0.0067	0.0059	0.0045	0.0029
Simulation	−0.0078	−0.0056	−0.0044	−0.0006
Theory	−0.0120	−0.0100	−0.0073	−0.0045
R	4.5	5.0	5.5	6.0
Simulation	−0.0044	−0.0036	−0.0030	−0.0033
Theory	−0.0073	−0.0057	−0.0045	−0.0037
d_N	4.0	5.0	6.0	8.0
Simulation	0.010	0.014	0.016	0.023
Theory	0.018	0.024	0.026	0.038

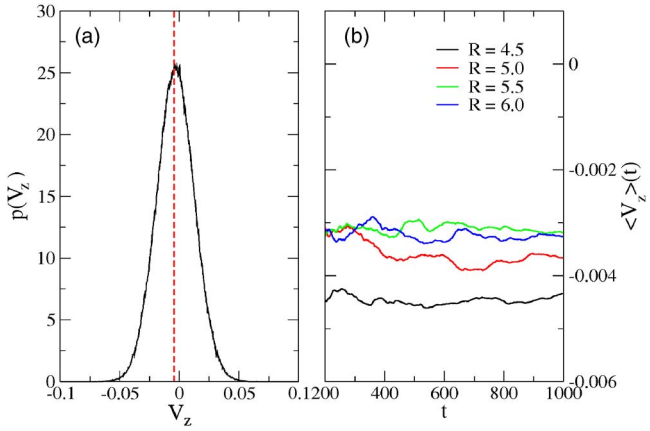

FIG. 4. (Color online) Probability distribution function (a) and time evolution of running averages (b) of the center-of-mass velocity of the nanodimer along its axis. The internuclear separation R ranges from 4.5 to 6.0. The dashed line in (a) indicates the mean velocity of the nanodimer with $R=4.5$. The repulsive LJ potential parameters are $\epsilon_A=1.0$ and $\epsilon_B=5.0$, respectively. Diameters of the catalytic and noncatalytic spheres are $d_C=d_N=4.0$ and the system temperature is $T=1/6$.

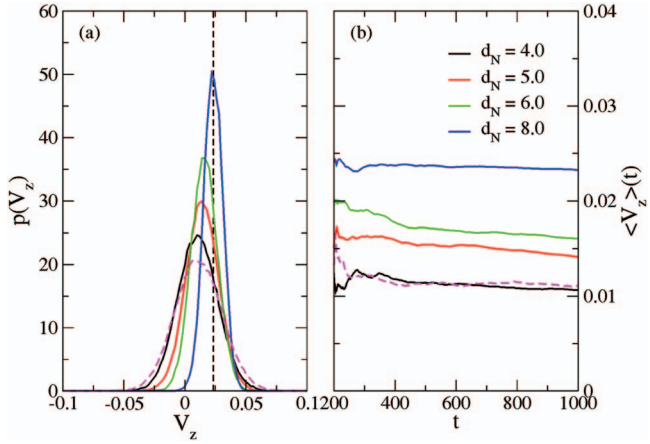

FIG. 5. (Color) Probability distribution functions (a) and time evolution of running averages (b) of the center-of-mass velocity of the nanodimer along its internuclear axis. The diameter of the catalytic sphere is d_C=4.0, while the noncatalytic sphere diameters are d_N=4.0, 5.0, 6.0, and 8.0, respectively. As a consequence, the corresponding internuclear separations are R=4.5, 5.1, 6.0, and 6.8. Energy parameters in all systems are ϵ_A=1.0 and ϵ_B=0.1, while the temperature is T=1/6. The dashed curves denote a system with d_C=3.0 and d_N=4.0.

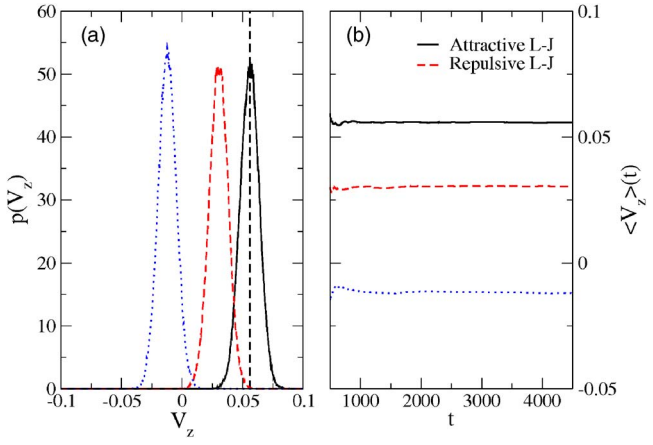

FIG. 6. (Color online) Probability distribution functions (a) and time evolution of running averages (b) of the center-of-mass velocity of the nanodimer along the internuclear axis. The solid and dashed curves correspond to systems in which B molecules interact with the noncatalytic sphere through attractive or repulsive LJ potentials, respectively. In these two examples the potential parameter are chosen to be equal ϵ_A=1.0 and ϵ_B=0.1. The dotted curves plot results for a system where repulsive LJ potentials with ϵ_B=5.0 exist between B solvent molecules and the N sphere. The system temperature is T=1/6, while diameters of the catalytic and the noncatalytic spheres are d_C=4.0 and d_N=8.0, respectively.

Figure 5 shows how V_z changes when the diameter of the noncatalytic sphere varies from 4.0 to 8.0. We chose energy parameters ϵ_A=1.0 and ϵ_B=0.1, so that the dimer moves with positive velocities as is expected for $\epsilon_B < \epsilon_A$ [Fig. 5(b)]. For d_N=8.0, the average velocity is somewhat larger than the peak width at half height of the Boltzmann distribution. Thus, the self-propelled motion of this nanodimer tends to dominate the thermal velocity fluctuations. As can be seen from Eq. (19), the average velocity V_z is proportional to σ_N^3, at given temperature and energy parameters. Thus, increasing the size of the noncatalytic sphere leads to a larger driving force for a fixed size of the catalytic sphere which is responsible for the production of B molecules. Increasing the size for the noncatalytic monomer of the nanodimer also increases the friction coefficient, but this increase is only roughly linear in the monomer sizes. Note that the velocity of a nanodimer with d_C=3.0 and d_N=4.0 [dashed curves in Fig. 5(b)] is not very different from that for a dimer with d_C=d_N=4.0, although the ratio of d_N/d_C is larger in the former case. Reducing the size of the catalytic sphere reduces the chemical reaction rate so that the nonequilibrium gradient in the A and B particle densities is smaller.

The force on the dimer varies strongly when the interaction potential between the noncatalytic sphere and the solvent B molecules changes from being repulsive to attractive. As the one can see from the results in Fig. 6(a), the directed dynamics of the nanodimer dominates Brownian motion. The simulated average velocities are found to be V_z=0.056 and 0.030 (the corresponding theoretical values are 0.175 and 0.043) for attractive and repulsive LJ potentials, respectively. The larger discrepancy between the theoretical and simulation results for attractive LJ potentials is likely due to errors in the steady state density field resulting from the neglect of the noncatalytic sphere. Any variation of the density field outside the interaction range is amplified by the attractive forces that act for distances smaller than r_c. Thus, the force estimate will be more sensitive to variations in the density field. Figure 6 also plots results for the nanodimer with ϵ_B=5.0. The dimer executes reverse directed motion in contrast to that for ϵ_B=0.1. Note that in our model, to construct a backward-moving nanodimer ($\epsilon_B > \epsilon_A$) using attractive LJ potentials between the noncatalytic sphere and solvent B molecules, the energy parameter ϵ must be chosen to be small enough to avoid a large accumulation of solvent B molecules around the nanodimer. However, weak interactions will lead to directed motion with smaller velocities and Brownian thermal fluctuations will again play an important role.

VI. CONCLUSION

The particle-based mesoscopic model for chemically powered self-propelled nanodimer dynamics discussed in this article provides insight into the factors that control the motion. Many synthetic molecular motors that have been fabricated have nanoscale dimensions.[13] Consequently, they operate in the presence of strong thermal fluctuations and descriptions of their propulsion mechanisms that rely on macroscopic concepts may not be valid. Our model couples the dimer motion to the solvent by intermolecular forces, which ultimately manifest themselves in properties such as the surface tension of macroscopic scales. The solvent dynamics preserves all conservation laws so that fluid flow and hydrodynamic interactions are automatically taken into account. The chemical reaction events that power the motor are also investigated at a microscopic level that incorporates both reaction-limited and diffusion-limited components to the rates. The simulations can be carried out under nonequilibrium steady state conditions so that statistical properties of the motion can be determined.

The important features that are often responsible for directed motion, asymmetry in the interactions and nonequilib-

rium chemical gradients, are easily identified in the model. The model is amenable to detailed theoretical analysis so that the specific geometrical and energetic factors that control the motion can be isolated and analyzed. This feature provides the basis for the design of chemically powered nanodimers whose velocities are larger that the velocity dispersion that results from thermal fluctuations. In this connection we see that an increase in size of the noncatalytic sphere that provides the motive force and manipulation of attractive versus repulsive interactions with this monomer can lead to large dimer velocities.

Since future uses of such self-propelled motors may find applications, for example, in directed synthesis and transport, it is essential to be able to construct motors whose dynamics does not simply result in enhanced diffusion but instead can be used to target objectives. We have considered only the simplest chemically powered nanodimer motors in the context of our mesoscopic framework. A variety of other translational and rotory motors can be constructed using similar methods.

ACKNOWLEDGMENTS

This research was supported in part by a grant from the Natural Sciences and Engineering Research Council of Canada.

[1] R. D. Vale and R. A. Milligan, Science **288**, 88 (2000).
[2] D. Pantaloni, C. Le Clainche, and M.-F. Carlier, Science **292**, 1502 (2001).
[3] A. Yildiz, J. N. Forkey, S. A. McKinney, T. Ha, Y. E. Goldman, and P. R. Selvin, Science **300**, 2061 (2003).
[4] E. M. Purcell, Am. J. Phys. **45**, 3 (1977).
[5] F. Jülicher, A. Ajdari, and J. Prost, Rev. Mod. Phys. **69**, 1269 (1997).
[6] V. Balzani, M. Gómez-López, and J. F. Stoddart, Acc. Chem. Res. **31**, 405 (1998).
[7] T. R. Kelly, Acc. Chem. Res. **34**, 514 (2001).
[8] J. Vicario, R. Eelkema, W. R. Browne, A. Meetsma, R. M. La Crois, and B. L. Feringa, Chem. Commun. (Camb.) 3936 (2005).
[9] R. Dreyfus, J. Baudry, M. L. Roper, M. Fermigier, H. A. Stone, and J. Bibette, Nature (London) **437**, 862 (2005).
[10] N. Mano and A. Heller, J. Am. Chem. Soc. **127**, 11574 (2005).
[11] R. Golestanian, T. B. Liverpool, and A. Ajdari, New J. Phys. **9**, 126 (2007).
[12] W. F. Paxton, S. Sundararajan, T. E. Mallouk, and A. Sen, Angew. Chem. Int. Ed. **45**, 5420 (2006).
[13] E. R. Kay, D. A. Leigh, and F. Zerbetto, Angew. Chem. Int. Ed. **46**, 72 (2007).
[14] J. M. Catchmark, S. Sundararajan, and A. Sen, Small **1**, 202 (2005).
[15] R. F. Ismagilov, A. Schwartz, N. Bowden, and G. M. Whitesides, Angew. Chem. Int. Ed. **41**, 652 (2002).
[16] W. F. Paxton, K. C. Kistler, C. C. Olmeda, A. Sen, S. K. St. Angelo, Y. Cao, T. E. Mallouk, P. E. Lammert, and V. H. Crespi, J. Am. Chem. Soc. **126**, 13424 (2004).
[17] S. Fournier-Bidoz, A. C. Arsenault, I. Manners, and G. A. Ozin, Chem. Commun. (Cambridge) 441 (2005).
[18] W. F. Paxton, A. Sen, and T. E. Mallouk, Chem. Eur. J. **11**, 6462 (2005).
[19] G. A. Ozin, I. Manners, S. Fournier-Bidoz, and A. C. Arsenault, Adv. Mater. **17**, 3011 (2005).
[20] T. R. Kline, W. F. Paxton, T. E. Mallouk, and A. Sen, Angew. Chem. Int. Ed. **44**, 744 (2005).
[21] P. Dhar, Th. M. Fischer, Y. Wang, T. E. Mallouk, W. F. Paxton, and A. Sen, Nano Lett. **6**, 66 (2006).
[22] J. R. Howse, R. A. L. Jones, A. J. Ryan, T. Gough, R. Vafabakhsh, and R. Golestanian, Phys. Rev. Lett. **99**, 048102 (2007).
[23] Y. Wang, R. M. Hernandez, D. J. Bartlett, Jr., J. M. Bingham, T. R. Kline, A. Sen, and T. E. Mallouk, Langmuir **22**, 10451 (2006).
[24] A. Najafi and R. Golestanian, Phys. Rev. E **69**, 062901 (2004).
[25] R. Golestanian, T. B. Liverpool, and A. Ajdari, Phys. Rev. Lett. **94**, 220801 (2005).
[26] D. C. Rapaport, Phys. Rev. Lett. **99**, 238101 (2007).
[27] D. J. Earl, C. M. Pooley, J. F. Ryder, I. Bredberg, and J. M. Yeomans, J. Chem. Phys. **126**, 064703 (2007).
[28] G. Rückner and R. Kapral, Phys. Rev. Lett. **98**, 150603 (2007).
[29] C. M. Pooley, G. P. Alexander, and J. M. Yeomans, Phys. Rev. Lett. **99**, 228103 (2007).
[30] A. Malevanets and R. Kapral, J. Chem. Phys. **110**, 8605 (1999).
[31] A. Malevanets and R. Kapral, J. Chem. Phys. **112**, 7260 (2000).
[32] A. Malevanets and R. Kapral, Lect. Notes Phys. **640**, 116 (2004).
[33] K. Tucci and R. Kapral, J. Chem. Phys. **120**, 8262 (2004).
[34] S. H. Lee and R. Kapral, J. Chem. Phys. **124**, 214901 (2006).
[35] T. Ihle and D. M. Kroll, Phys. Rev. E **63**, 020201 (2001).
[36] T. Ihle and D. M. Kroll, Phys. Rev. E **67**, 066705 (2003).
[37] D. Frenkel and B. Smit, *Understanding Molecular Simulation—From Algorithms to Applications* (Academic, San Diego, 1996).
[38] H. C. Andersen, J. Comput. Phys. **52**, 24 (1983).
[39] B. J. Alder and T. E. Wainwright, Phys. Rev. A **1**, 18 (1970).
[40] S. H. Lee and R. Kapral, J. Chem. Phys. **121**, 11163 (2004).
[41] J. Happel and H. Brenner, *Low Reynolds Number Hydrodynamics* (Nijhoff, Dordrecht, 1965).
[42] S. H. Lee and R. Kapral, J. Chem. Phys. **122**, 214916 (2005).
[43] N. Kikuchi, C. M. Pooley, J. F. Ryder, and J. M. Yeomans, J. Chem. Phys. **119**, 6388 (2003).
[44] M. Ripoll, K. Mussawisade, R. G. Winkler, and G. Gompper, Phys. Rev. E **72**, 016701 (2005).
[45] R. Kapral, Adv. Chem. Phys. **48**, 71 (1981).